



Bound states in the continuum and long-lived electronic resonances in mesoscopic structuresLeonard Dobrzyński *Institut d'Electronique, de Microélectronique et de Nanotechnologie, UMR Centre National de la Recherche Scientifique 8520, Département de Physique, Université de Lille, 59655 Villeneuve d'Ascq Cédex, France*Housni Al-Wahsh *Engineering Mathematics and Physics Department, Faculty of Engineering, Benha University, Shoubra 11629, Cairo, Egypt and Institut d'Electronique, de Microélectronique et de Nanotechnologie, UMR Centre National de la Recherche Scientifique 8520, Département de Physique, Université de Lille, 59655 Villeneuve d'Ascq Cédex, France*Abdellatif Akjouj *Institut d'Electronique, de Microélectronique et de Nanotechnologie, UMR Centre National de la Recherche Scientifique 8520, Département de Physique, Université de Lille, 59655 Villeneuve d'Ascq Cédex, France*Eman A. Abdel-Ghaffar *Electrical Engineering Department, Faculty of Engineering, Benha University, Shoubra 11629, Cairo, Egypt*

(Received 19 February 2024; revised 1 July 2024; accepted 10 July 2024; published 26 July 2024)

A. bound state eigenfunction is defined here to be strictly localized within a subspace of the structure under study and has no decreasing behavior. Its eigenwavelength can be within state continua. Bound states in the continuum (BICs) and long-lived resonances have become a unique way to produce the extreme localization of electronic waves. We present a theoretical and numerical demonstration of semi-infinite bound states in the continuum (SIBICs) and long-lived resonances in a ringlike electronic microresonator coupled to a finite stub and to two electronic rib/ridge waveguides, together with their existence conditions. This structure is composed of a closed loop of length L , a finite stub of length L_1 and two semi-infinite leads. SIBICs localized in a semi-infinite subspace domain induce transmission zeros. Others induce transmission ones in the middle of long-lived resonances. The BICs correspond to localized resonances of infinite lifetime inside the structure, without any leakage into the surrounding leads. When BICs exist within state continua, they induce Fano resonances exhibiting sharp peaks in the transmission spectra and in the variation of the density of states for specific values of the stub length L_1 . This enables one to regulate these resonances by means of this length. The obtained results take due account of the state number conservation between the final system and the reference one. This conservation rule enables one to find all the states of the final system and among them the bound in the continuum ones. The analytical results are obtained by means of the Green's function technique. The structures and the long-lived resonances presented in this paper may have potential applications due to their high sensitivities to weak perturbations, in particular in sensing, wave filtering, and microelectronic devices.

DOI: [10.1103/PhysRevB.110.035428](https://doi.org/10.1103/PhysRevB.110.035428)**I. INTRODUCTION**

Classical and quantum finite systems have discrete states. A bound state eigenfunction is defined to be strictly localized within a subspace of a system. Its eigenvalue can be within state continua. Without dissipation, the states have an infinite lifetime. A discrete state in interaction with a state continuum induces at least one resonance. It may also remain bound within a finite subspace, and become a bound state in the continuum (BIC) [1]. When such a resonance has an infinite lifetime, it is a discrete state. When its frequency passing band is confined by one or two zeros of transmission, it is a long-lived resonance [2–5].

Recently bound states in the continuum, also known as trapped modes, have enabled researchers to create systems with long-lived resonances in order to enhance photon-

matter interaction [6]. A BIC manifests itself as a resonance with zero linewidth in lossless systems. It exists within the state continua but remains perfectly confined in some parts of the system (subsystem). BICs were first predicted by Neumann and Wigner in 1929 [1]. Since then, BICs were found in various fields of physics such as electronics [7,8], photonics [9–12], acoustics [13,14], magnonics [15], and plasmonics [16–18]. Interest in BICs also results from their potential use in many applications such as lasers [19], filters [20,21], and sensors [22,23]. BICs can be classified into several mechanisms related to their discovery origin [6], e.g., symmetry-protected BICs [24–27], accidental BICs [28–30], Fabry-Pérot BICs [31–33] and Friedrich-Wintgen BICs [34–37] which have been subsequently investigated theoretically and experimentally in different physical systems

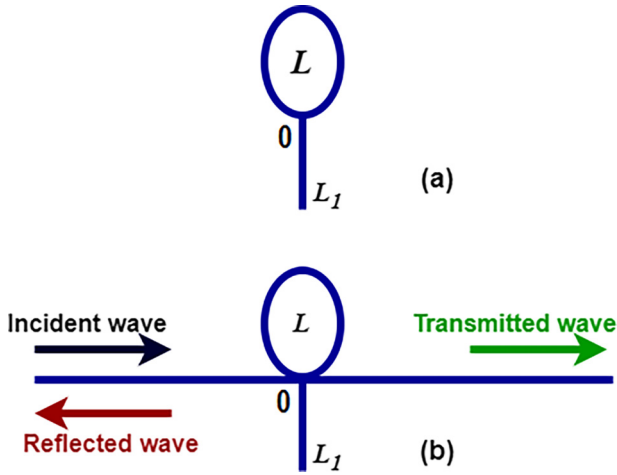


FIG. 1. The simple structure studied in this paper. The structure made out of two guides of lengths L and L_1 . When closing the L one at space point zero, one connects to the zero end of the guide of length L_1 (a). Finally two semi-infinite leads are connected to the space point zero (b). The space point zero is the point of connection of the two semi-infinite leads with the two guides, L and L_1 , constituting the structure. This is why we call it the *interface point*. The *interface space* for this structure is the point zero. This interface space is written shortly as $M = \{0\}$.

[38–42]. Let us also mention that very recently researchers discovered another type of BICs called momentum-mismatch-driven BICs [43]. BICs are not observable from the spectrum due to their nonradiative property with vanishing spectral linewidth. However, they can exist only under a specific choice of the material or geometrical parameters of the system. Thus, by slightly detuning the system from the BIC conditions (e.g., changing the geometrical parameters), the BIC induces a long-lived resonance with a finite width.

No state can interact with another one through an eigenfunction zero [44–46]. With the leads, some final states may be, in the present paper, BICs, or semi-infinite bound states in the continuum (SIBICs). BICs or SIBICs are bound respectively in finite or infinite system subspaces. They are induced by their eigenfunction zeros and the fact that they cannot interact with any other state through these robust zeros [44]. This paper reports SIBIC inducing transmission zeros and after detuning the geometrical parameters of the structure long-lived resonances. It presents also SIBICs inducing directly transmission ones and long-lived resonances. These results are reported here for a one-dimensional (1D) electronic structure composed of one closed loop attached to a stub and two semi-infinite leads [see Fig. 1(b)].

These results are obtained by means of the interface response theory [47] which enables one also to deduce the state phase shifts, the variation of the density of states (VA-DOS), the transmission rate, the transmission phase, and the transmission phase time. These results take due account of the state number conservation between the final system and the reference one constituted by the independent closed loop, stub, and semi-infinite leads. This conservation rule enables one to find all the states of the final system and in particular the bound ones [45].

The rest of the paper is organized as follows: In Sec. II we present a detailed theoretical study of a one-dimensional system. The aim of this section is to present the inverse surface Green's function elements of the elementary constituents of the waveguide structure studied in this paper using interface response theory. Section III gives the final state results obtained for the structure presented in Fig. 1(a). Transmission, reflection, BICs, SIBICs, and Fano resonance are presented in Sec. IV. Section V gives the results obtained for the transmission phase and the state phase shift. The summary and perspective are presented in Sec. VI.

II. INTERFACE RESPONSE THEORY OF CONTINUOUS MEDIA

A. Overview

In this paper, we study the propagation of electronic waves in composite systems composed of one-dimensional continuous finite guides grafted on different semi-infinite guides. This paper is performed with the help of the interface response theory [47] of continuous media which permits us to calculate the Green's function of any composite material. In what follows, we present the basic concepts and the fundamental equations of this theory.

Let us consider any composite material contained in its space of definition D and formed out of N different homogeneous pieces situated in their domains D_i . Each piece is bounded by an interface M_i , adjacent in general to j ($1 < j < J$) other pieces through subinterface domains M_{ij} . The ensemble of all these interface spaces M_i will be called the interface space M of the composite material.

The elements of the Green's function $g(DD)$ of any composite material can be obtained from [47]

$$g(D, D) = G(D, D) - G(D, M)G^{-1}(M, M)G(M, D) + G(D, M)G^{-1}(M, M)g(M, M)G^{-1}(M, M)G(M, D), \quad (1)$$

where $G(DD)$ is the Green's function of a reference continuous medium and $g(MM)$ denotes the interface elements of the Green's function of the composite system. The inverse $g^{-1}(MM)$ of $g(MM)$ is obtained for any points in the space of the interfaces $M = (\sqcup M_i)$ as a superposition of the different $g_i^{-1}(M_i, M_i)$ [47] inverse of the $g_i(M_i, M_i)$ for each constituent i of the composite system. The latter quantities are given by the equation

$$g_i^{-1}(M_i, M_i) = \Delta_i(M_i, M_i)G_i^{-1}(M_i, M_i), \quad (2)$$

where

$$\Delta_i(M_i, M_i) = I(M_i, M_i) + A_i(M_i, M_i), \quad (3)$$

where I is the unit matrix and

$$A_i(x, x') = V_i(x'')G_i(x'', x')|_{x''=x}, \quad (4)$$

where $x, x'' \in M_i$ and $x' \in D_i$.

In Eq. (4), the cleavage operator V_i acts only in the surface domain M_i of D_i and cuts the finite or semi-infinite size block

out of the infinite homogeneous guide [47]. A_i is called the surface response operator of guide i .

The new interface states can be calculated from [47]

$$\det[g^{-1}(M, M)] = 0, \quad (5)$$

showing that, if one is interested in calculating the interface states of a composite, one only needs to know the inverse of the Green's function of each individual block in the space of their respective surfaces and/or interfaces.

Moreover, if $U(D)$ represents an eigenvector of the reference system, Eq. (1) enables one to calculate the eigenvectors $u(D)$ of the composite material [47]:

$$\begin{aligned} u(D) = & U(D) - U(M)G^{-1}(M, M)G(M, D) \\ & + U(M)G^{-1}(M, M)g(M, M)G^{-1}(M, M)G(M, D). \end{aligned} \quad (6)$$

In Eq. (6), $U(D)$, $U(M)$, and $u(D)$ are row vectors. Equation (6) enables one also to calculate all the waves reflected and transmitted by the interfaces as well as the reflection and the transmission coefficients of the composite system. In this case, $U(D)$ must be replaced by an incident wave launched in one homogeneous piece of the composite material.

B. Inverse surface Green's function elements of the elementary constituents

We report here the expression of the Green's function of a homogeneous isotropic infinite medium. For the sake of simplicity, we restrict ourselves to homogeneous guides. We give also the inverse of the surface Green's function for the semi-infinite guide with a free surface and for the finite guide of length L .

1. Green's function of an infinite guide

We describe the electronic propagation in the frame of a free particle model in which $E = (\hbar^2 k^2 / 2m) + V$, where m , V , and k refer respectively to the effective mass, a constant potential, and a wave vector.

In this paper, we focus on homogeneous structures where all media (the loop, the side resonator, and the semi-infinite leads; see Fig. 1) are made of the same material, namely, GaAs. The material parameters are then $V = 0.0$ meV and $m = 0.067 m_0$, where m_0 is the free electron mass.

The time independent Schrödinger equation for standing electronic waves is [48]

$$\left(\frac{d^2}{dx^2} - k^2 \right) \psi(x) = 0, \quad (7)$$

where x is the space position along the structure and $k = \frac{1}{\hbar} \sqrt{2mE}$. The response function $G(x, x')$ of this infinite guide is defined by

$$\left(\frac{d^2}{dx^2} - k^2 \right) G(x, x') = \delta(x - x'), \quad (8)$$

where δ stands for the Dirac delta distribution, also known as the unit impulse. The corresponding response function is

$$G(x, x') = \frac{e^{ik|x-x'|}}{2ik} \quad (9)$$

where $i = \sqrt{-1}$.

2. Semi-infinite guide

One considers a semi-infinite guide with a “free surface” located at the position $x = 0$ in the direction Ox of the Cartesian coordinates. The end of a semi-infinite guide is treated as a perturbation of the infinite guide. Within this approach, one defines first the surface cleavage operator which is the perturbation

$$V_s(x) = \delta(x) \frac{d}{dx} \quad (10)$$

where $\delta(x)$ is the Dirac function indicating that this perturbation acts only at the point x , where the infinite guide is cleaved into two semi-infinite ones. This cleavage operator creates two semi-infinite guides with free ends.

Then one can define the surface response operator

$$A_s(x, x') = V_s(x'')G(x'' - x'), \quad (11)$$

for $x'' = x$. In this expression, x takes only the semi-infinite guide zero end value.

Then one obtains

$$A_s(x, x') = -\frac{1}{2}. \quad (12)$$

The response function for each semi-infinite guide can then be found, using the corresponding truncated part of G . For the semi-infinite guide such that $x \geq 0$, one finds

$$g_s(x, x') = \frac{1}{2ik} \{ \exp(ik|x-x'|) + \exp[ik(x-x')] \}. \quad (13)$$

The inverse of the surface Green's function of a semi-infinite guide at the surface point $x = x' = 0$ is given by

$$g_s^{-1}(M, M) = g_s^{-1}(0, 0) = ik. \quad (14)$$

3. Finite guide

One considers a finite guide of length L bounded by two free surfaces located at $x = 0$ and L in the direction Ox of the Cartesian coordinates system. In this case [49]

$$g_L^{-1}(M, M) = \frac{k}{S} \begin{pmatrix} -C & 1 \\ 1 & -C \end{pmatrix} = \begin{pmatrix} g_L^{-1}(0, 0) & g_L^{-1}(0, L) \\ g_L^{-1}(L, 0) & g_L^{-1}(L, L) \end{pmatrix} \quad (15)$$

where $C = C(L) = \cos(kL)$ and $S = S(L) = \sin(kL)$. One can see that in the interface domain M corresponding to interfaces $x = 0$ and L , the surface Green's function is a 2×2 square matrix. In order to study elementary excitation, we calculate the surface Green's function for different composite systems composed of finite segments grafted on a one-dimensional wave guide.

The matrix inverse of $[g(M, M)]^{-1}$, namely,

$$g(M, M) = \frac{1}{kS} \begin{pmatrix} C & 1 \\ 1 & C \end{pmatrix}, \quad (16)$$

is the interface response matrix. The elements of this matrix give the interface response functions $g(0, 0) = g(L, L) = C/(kS)$, $g(0, L) = g(L, 0) = 1/(kS)$.

4. One loop

A monomode guide of length L is an important elementary brick out of which almost any linear material, device, and system may be built out. It is also a good example for learning the general method enabling one to construct new systems out of finite guides. When closing the finite guide by superposing its ends zero and L [see Fig. 1(a)], the inverse of the interface response function on the connection point [using Eq. (16)] is given by

$$g^{-1}(0, 0) = -2k \frac{C}{S} + 2k \frac{1}{S} = 2k \frac{S(L/2)}{C(L/2)}. \quad (17)$$

III. ONE LOOP L AND ONE STUB L_1 STATES

Consider now a reference system made out of two guides of lengths L and L_1 . When closing the L one at space point zero, one connects to it the zero end of the guide L_1 [see Fig. 1(a)]. One obtains for this system, without the semi-infinite leads, instead of Eq. (17)

$$\begin{aligned} [g(0, 0)]^{-1} &= k \left(\frac{2S(L/2)}{C(L/2)} + \frac{S(L_1)}{C(L_1)} \right) \\ &= k \left(\frac{2S(L/2)C(L_1) + C(L/2)S(L_1)}{C(L/2)C(L_1)} \right). \end{aligned} \quad (18)$$

For each finite guide of length L , the discrete states are given by the poles of the Green's function, namely $kS(L) = 0$ [see Eq. (16)], therefore the initial states of the system composed of the two independent guides (the loop of length L and the stub of length L_1) are given by $[kS(L)][kS(L_1)] = 0$. We have also for each finite guide [using Eq. (15)] that the determinant of the surface Green's function is given by $|g_L^{-1}(M, M)| = -k^2$. For the stub of length L_1 [using similar procedure for the calculation of the element $g(0, 0)$ of Eq. (16)] we get $|g_L^{-1}(0, 0)| = kS(L_1)/C(L_1)$. Therefore, for the reference system presented in Fig. 1(a) $g_R^{-1}(0, 0) = (-k^2)[kS(L_1)/C(L_1)] = -k^3S(L_1)/C(L_1)$.

So the final states of the structure presented in Fig. 1(a) are given by the state number conservation and the state phase shift [45] to be

$$[kS(L)][kS(L_1)] | [g(0, 0)]^{-1} | \left[\frac{1}{-k^3S(L_1)/C(L_1)} \right] = 0, \quad (19)$$

that is,

$$S(L/2)[2S(L/2)C(L_1) + C(L/2)S(L_1)] = 0. \quad (20)$$

When $L/2$ and L_1 are commensurate, it is possible to factorize the last term in the above equation with the help of the Chebyshev polynomials. If $L_1 = 0$ we get the two degenerate closed loop states, namely $S^2(L/2) = 0$. Let us stress that these discrete states are two times degenerate. Their respective standing wave eigenfunctions are $\cos(kx)$ and $\sin(kx)$, where x is an arbitrary space point of the reference guide of length L . For $x = 0$, the first eigenfunction has the value 1 and the second one has the value zero. One independent infinite lead has also these standing state eigenvalues and these eigenfunctions, but within other bounds. So in one independent infinite lead the $\sin(kx)$ state is a hidden state in the continuum of the states of its twin $\cos(kx)$ one [44]. It is also the eigenfunction of a hidden discrete state within the loop.

Equations (18) and (20) enable us to find the eigenvector values u for particular states of the final system from

$$[g(0, 0)]^{-1} u = 0. \quad (21)$$

For the states defined by $S(L/2) = 0$, i.e., $kL/2\pi = n$, where $n = 0, 1, 2, \dots$ we get $u = 0$ when $S(L_1) \neq 0$ and $u = 1$ when $S(L_1) = 0$, i.e., $kL/2\pi = (n/2)(L/L_1)$. This last possibility happens only when L and L_1 are commensurate. For the $[2S(L/2)C(L_1) + C(L/2)S(L_1)] = 0$ states, we get $u = 1$. For the states defined by $C(L/2) = 0$, i.e., $kL/2\pi = n + (1/2)$, where $n = 0, 1, 2, \dots$ we get $u = 0$. For the states defined by $C(L_1) = 0$, i.e., $kL/2\pi = [(2n + 1)/4](L/L_1)$, where $n = 0, 1, 2, \dots$ we get $u = 0$.

According to the above results and to the BIC and SIBIC theorems given in our previous work [50], once the two leads are connected [Fig. 1(b)], the above eigenvector zeros are the signatures of BIC or SIBIC and transmission zeros. Note also that the eigenvector ones are for this system, the signatures of transmission ones, falling in between the transmissions zeros and being then the tops of long-lived resonances.

IV. TRANSMISSION AND REFLECTION

The structure presented in Fig. 1(b) is composed of a loop of length L and a stub of length L_1 , inserted between two semi-infinite leads. The inverse of the Green's function of the whole system is given by a linear superposition of the Green's functions of its constituents given above [Eqs. (14) and (18)] in the interface space $M = \{0\}$, namely [51],

$$[g(0, 0)]^{-1} = k \left(\frac{2S(L/2)C(L_1) + C(L/2)S(L_1)}{C(L/2)C(L_1)} + 2i \right). \quad (22)$$

Let us consider an incident wave $U(x) = e^{-ikx}$ launched in the left semi-infinite lead [Fig. 1(b)]. From Eq. (22), one can obtain the transmission coefficient in the right semi-infinite lead, namely, $t = -2ikg(0, 0)$, or equivalently

$$t = \frac{-2iC(L/2)C(L_1)}{2S(L/2)C(L_1) + S(L_1)C(L/2) + 2iC(L/2)C(L_1)}. \quad (23)$$

The transmittance $T(=|t|^2)$ is

$$T = \frac{4C^2(L/2)C^2(L_1)}{[2S(L/2)C(L_1) + S(L_1)C(L/2)]^2 + 4C^2(L/2)C^2(L_1)}. \quad (24)$$

In the same way, the reflection coefficient in the left semi-infinite lead is given by $r = -1 + 2ikg(0, 0)$ and the reflectance $R(=|r|^2)$ is

$$R = \frac{[2S(L/2)C(L_1) + S(L_1)C(L/2)]^2}{[2S(L/2)C(L_1) + S(L_1)C(L/2)]^2 + 4C^2(L/2)C^2(L_1)}. \quad (25)$$

From Eqs. (24) and (25), one can easily check (in the absence of loss) the conservation law $R + T = 1$.

A. Bound states in the continuum

The loop and stub structure (Fig. 1) can exhibit BICs and Fano resonances. BICs are described as resonances with zero

widths in the transmission and density of states spectra. These states can occur only under specific geometrical lengths L and L_1 . When departing slightly from the BIC conditions, they transform to specific Fano or electromagnetic induced transparency (EIT) resonances that are characterized by a zero Fano parameter.

It is well known that the eigenmodes of the structure presented in Fig. 1(b) are given by the poles of the transmission coefficient t [Eq. (23)] or equivalently by the poles of the Green's function [Eq. (22)], namely,

$$2S(L/2)C(L_1) + S(L_1)C(L/2) + 2iC(L/2)C(L_1) = 0. \quad (26)$$

The above equation is a complex quantity. Its real part gives the position of the resonances in transmission and density of states, whereas its imaginary part is related to the width of the resonance and also here to the transmission active states. In general, it is not easy to simultaneously cancel the real and imaginary parts of this equation at the same frequency. This will correspond to a bound state falling in the continuum of states. In order to avoid the divergence of t , then its numerator should also vanish in such a way that t becomes finite. These two conditions can be fulfilled only if $C(L/2) = 0$ and $C(L_1) = 0$. A simple algebra leads to the following condition:

$$\frac{(L/2)}{L_1} = \frac{p}{q}, \quad (27)$$

where p and q are odd numbers. This leads to the conclusion that L and L_1 should be commensurate with each other.

Let us define a unit length L_0 such that the loop length L and the stub length L_1 are multiples of L_0 (i.e., $L/2 = pL_0$ and $L_1 = qL_0$). Therefore Eq. (26) can be written as

$$2S(pL_0)C(qL_0) + S(qL_0)C(pL_0) + 2iC(pL_0)C(qL_0) = 0 \quad (28)$$

or equivalently

$$2S(pL_0)T_q(C_0) + S(qL_0)T_p(C_0) + 2iT_p(C_0)T_q(C_0) = 0. \quad (29)$$

Here, T_p and T_q are the Chebyshev polynomials of the first kind, and $C_0 = C(L_0) = \cos(kL_0)$. Since p and q are odd numbers, one can factorize $C(L_0)$ out of each term of the above equation, i.e., Eq. (29) can be written as

$$C_0[2S(pL_0)T_q'(C_0) + S(qL_0)T_p'(C_0) + 2iC_0T_p'(C_0)T_q'(C_0)] = 0, \quad (30)$$

where $T_p(C_0) = C_0 T_p'(C_0)$ and $T_q(C_0) = C_0 T_q'(C_0)$. Therefore the BICs are given by $C_0 = \cos(kL_0) = 0$, i.e.,

$$\frac{kL}{2\pi} = \frac{(2n+1)}{2}p, \quad (31)$$

where $n = 0, 1, 2, \dots$. Therefore for each pair of (n, p) we will have a BIC (see Fig. 2).

B. Semi-infinite bound states in the continuum

Another effect is that each of the loop L and the stub L_1 may create one SIBIC when a lead is attached to the port zero. Equation (22) [or equivalently Eq. (23)] enables one to conclude that for $C(L_1) = 0$ and for $C(L/2) = 0$ the eigenfunctions vanish on the port zero, which in turn induce transmission zeros. The one corresponding to $C(L/2) = 0$ is

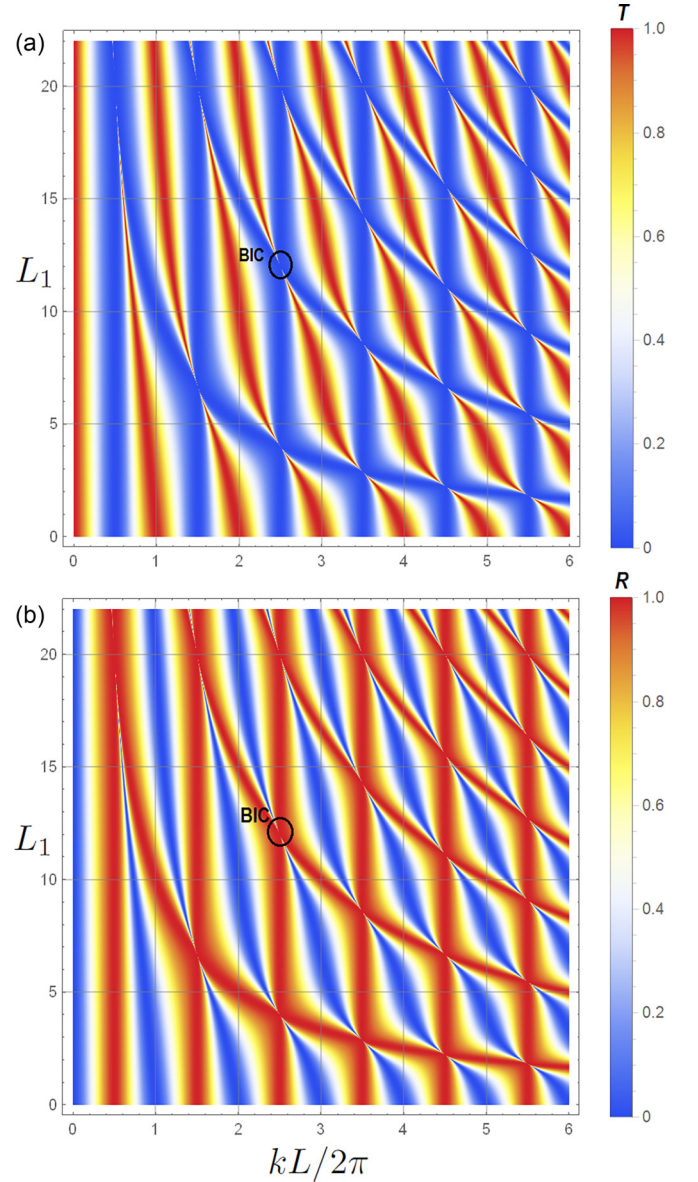


FIG. 2. For the structure presented in Fig. 1(b) the above plots shows the variation of transmittance (a) and reflectance (b) (with color scale) vs the reduced wave vector $kL/2\pi$ and the stub length L_1 . The loop length is considered to be $L = 40$ nm. For each pair of (n, p) we get a value for $kL/2\pi$ [Eq. (31)] where BICs exist for several values of the stub length L_1 [vertical blue lines in (a) or vertical red lines in (b)]. For example, if $p = 1$, then the BICs will appear [using Eq. (31)] at $kL/2\pi = 1/2, 3/2, 5/2, \dots$. If in addition $q = 1$, i.e., $L_1 = L/2 = 20$ nm [see Eq. (27)], the BICs appear at $(kL/2\pi, L_1) = (1/2, 20), (3/2, 20), (5/2, 20), \dots$. The black circles represent, for example, the BIC appearing at $(kL/2\pi, L_1) = (5/2, 12)$.

a SIBIC localized in one semi-infinite lead and in the loop L . Similarly, the one corresponding to $C(L_1) = 0$ is a SIBIC localized in one semi-infinite lead and in the stub L_1 . When this happens for different eigenwave vectors, this system has two SIBICs. When this happens for the same wave vector, L_1 should be commensurate with $L/2$. In such case these SIBIC states may induce BICs (see for example Fig. 2 for

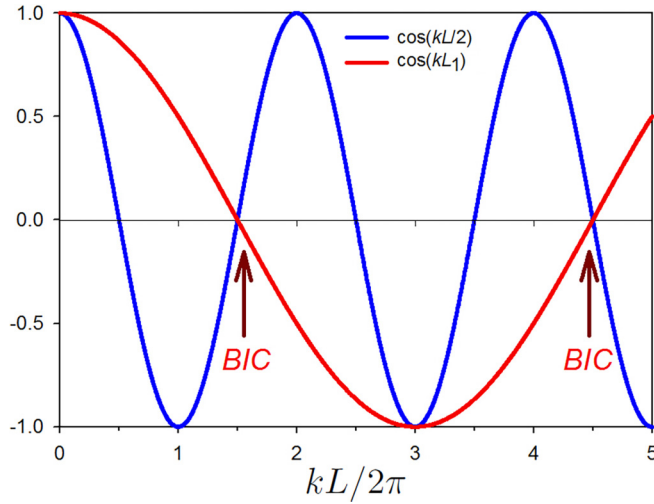


FIG. 3. Illustrative example for the existence of the BICs due to the intersection of the curves given by $\cos(kL_1) = 0$ and $\cos(kL/2) = 0$. The parameters used for this plot are $L = 40$ nm, $L_1 = L/6$. The BICs appear [using Eqs. (27) and (31) for $p = 3$, $q = 1$] at $(kL/2\pi, L_1) = (3/2, 40/6), (9/2, 40/6), \dots$ (see Fig. 2).

the case where $L_1 = L/2$). These SIBICs and BICs induce transmission zeros (important for the long-lived resonance creations).

Let us stress that for the eigenstates given by the zeros of the real part of the denominator of Eq. (23), we get $t = 1$. So there are transmission ones between the transmission zeros provided by the $C(L_1) = 0$ and the $C(L/2) = 0$ SIBICs. Therefore this system shows long-lived resonances for any incommensurate or commensurate values of L_1 and L .

Figures 2(a) and 2(b) give, respectively, the variation of the transmittance and reflectance (with color scale) versus the reduced wave vector $kL/2\pi$ and the stub length L_1 . One can observe that for each pair (n, p) , BICs occur for $kL/2\pi = (2n + 1)p/2$. These BICs appear as the intersection of the curves given by $\cos(kL_1) = 0$ and $\cos(kL/2) = 0$ (see Fig. 3). One can also notice that at these points the transmission (reflection) is completely zero (one). In fact, the BICs have robust zeros at port zero. In order to make these BICs pop out as a sharp long-lived resonance when plotting the transmission curve we have to break the symmetry of the structure shown in Fig. 1(b) by increasing/decreasing the stub length L_1 . Figure 2(a) shows how the width of these resonances can be tuned using the stub length L_1 . The color code given on the right enables one to understand how this resonance increase/decreases in function $kL/2\pi$.

In order to give a better understanding about the behavior of the SIBICs, BICs, and the associated Fano resonances in the transmission coefficient, we will focus, in what follows, on the BIC associated to the pair $(n = 0, p = 5)$ and $q = 3$, i.e., at $(kL/2\pi, L_1) = (5/2, 12)$ [see Fig. 2(a)]. In Fig. 4 we plot a zoom of the variation of transmittance [Fig. 4(a)] and reflectance [Fig. 4(b)] (with color scale) versus $kL/2\pi$ and the stub length L_1 . The black circles represent the BIC position. One can notice the narrowing of the resonance, then its transformation into a BIC at $(kL/2\pi, L_1) = (5/2, 12)$ nm). A transparency window between two zeros (induced by the

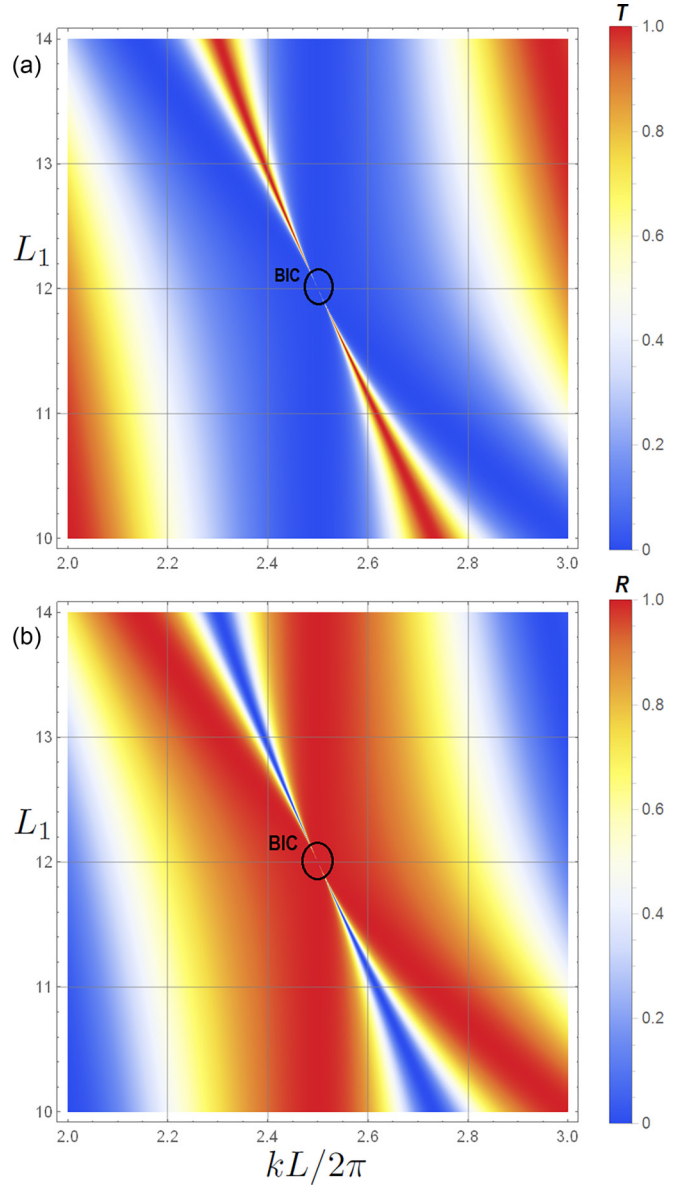


FIG. 4. For the structure presented in Fig. 1(b) the plots show a zoom of the variation of transmittance (a) and reflectance (b) (with color scale) vs the reduced wave vector $kL/2\pi$ and the stub length L_1 . The loop length is considered to be $L = 40$ nm. In this plot we are focusing on the BIC associated to the pair $(n = 0, p = 5)$ and $q = 3$, i.e., at $(kL/2\pi, L_1) = (5/2, 12)$. The black circles represent the BIC position. One can notice the narrowing of the resonance, then its transformation into a BIC at $(kL/2\pi, L_1) = (5/2, 12)$. A transparency window between two zeros (induced by the SIBICs) appears when we deviate slightly from the BIC condition, giving rise to electronic induced transparency resonance.

SIBICs) appears when we deviate slightly from the BIC condition, giving rise to electronic induced transparency resonance.

In addition we plotted in Figs. 5(a), 5(c), and 5(e) the transmittance in function $kL/2\pi$ for three values of L_1 , namely $L_1 = 12.25, 12$, and 11.75 nm respectively. The peak between the transmission zeros given by the two SIBICs $C(L_1) = 0$ and $C(L/2) = 0$ [denoted by dark red arrows in Figs. 5(b)

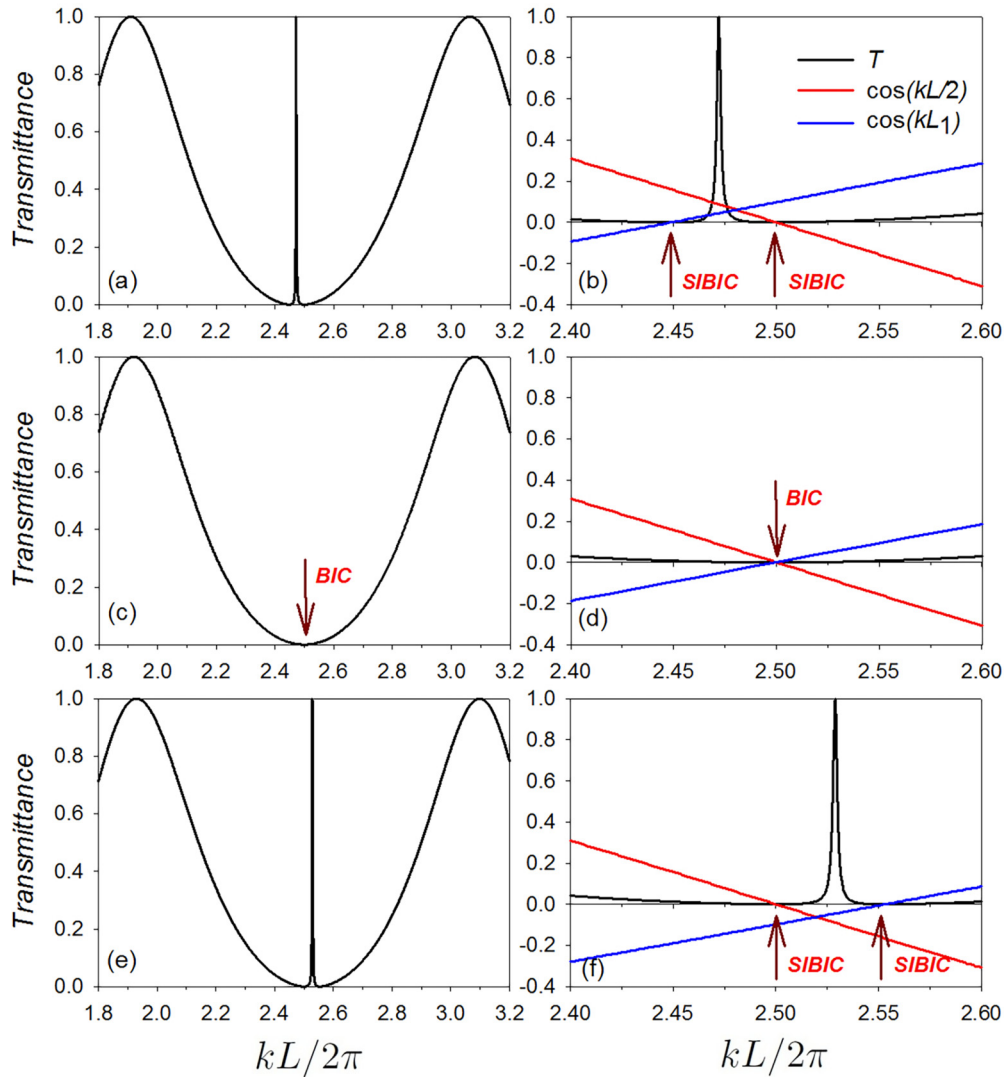


FIG. 5. For the structure presented in Fig. 1(b) the plots in (a), (c), and (e) show the variation of transmittance vs the reduced wave vector $kL/2\pi$ for three values of the stub length L_1 , namely $L_1 = 12.25$, 12 , and 11.75 nm respectively. The length of the loop L is considered to be 40 nm. In this figure we are focusing on the BIC associated to the pair $(n = 0, p = 5)$ and $q = 3$, i.e., at $(kL/2\pi, L_1) = (2.5, 12 \text{ nm})$. The peak between the transmission zeros given by the two SIBICs [provided by $C(L_1) = 0$ and $C(L/2) = 0$ and denoted by dark red arrows in (b) and (f)] gives rise to a well defined (EIT) resonance. This resonance becomes narrow as L_1 decreases (increases) down (up) to 12 nm. At $L_1 = 12$ nm the width of this resonance disappears, giving rise to the BIC at $kL/2\pi = 2.5$ [denoted by dark red arrows in (c) and (d)].

and 5(f) gives rise to a well defined EIT resonance. This resonance becomes narrow as L_1 decreases (increases) down (up) to 12 nm. At $L_1 = 12$ nm the width of this resonance disappears, giving rise to a BIC at $kL/2\pi = 5/2$ [denoted by dark red arrows in Figs. 5(c) and 5(d)]. The BIC transforms to a quasi-BIC as we shift out from the BIC position. In general, the quasi-BIC manifests itself as a Fano resonance in the transmission and a narrow resonance in the VADOS (see below).

Figure 6 represents a zoomed view for the transmittance (black line) and reflectance (red line) versus the reduced wave vector $kL/2\pi$ for the resonance given in Fig. 5(a) [or Fig. 5(b)]. The parameters are $L = 40$ nm and $L_1 = 12.25$ nm. One can notice that the loop and the stub interfere destructively (constructively), giving rise to a zero reflection (total transmission). This result is in accordance with the conservation law $R + T = 1$ and the discussion

given above where the total transmission occurs between two transmission zeros induced by the two SIBICs provided by $C(L_1) = 0$ and $C(L/2) = 0$. This result can be qualified as EIT resonance.

Figure 7 shows the variation of the transmittance (black line) and reflectance (red line) versus the stub length L_1 at $kL/2\pi = 3$ and $L = 40$ nm. One can see that with increasing the value of the stub length L_1 the transmittance (reflectance) varies periodically between zero and one. There is also some values of L_1 where the transmittance and reflectance are equal. These results show that the peaks in the transmittance (reflectance) can be controlled by detuning the length of the stub.

C. Fano resonance

The resonance in Fig. 5(a) shows the same characteristics as a Fano resonance but with two zeros (due to the two

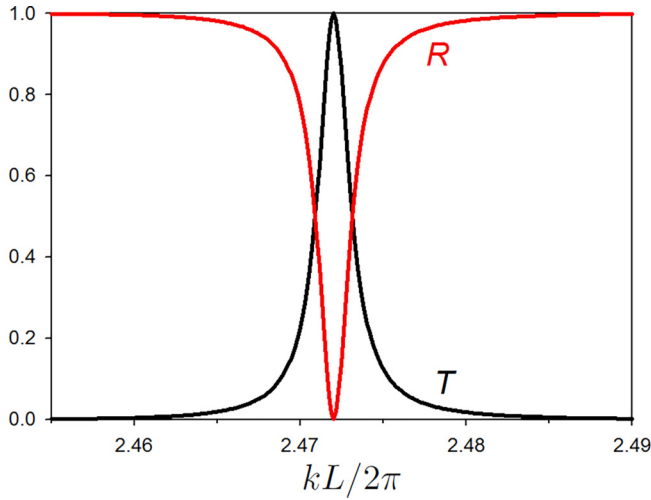


FIG. 6. A zoomed view of the transmittance (black line) and reflectance (red line) vs $kL/2\pi$ for the resonance given in Fig. 5(a) [or Fig. 5(b)]. The parameters are $L = 40$ nm and $L_1 = 12.25$ nm. Notice that the loop and the stub interfere destructively (constructively), giving rise to a zero reflection (total transmission). This result is in accordance with the conservation law $R + T = 1$. Note also that the total transmission occurs between two transmission zeros induced by the two SIBICs provided by $C(L_1) = 0$ and $C(L/2) = 0$. This result can be qualified as EIT resonance.

SIBICs) of transmission around the resonance instead of 1, as is usually the case. Indeed, one can obtain an approximate analytical expression for the transmission coefficient [Eq. (23)] in the vicinity of the resonance. A Taylor expansion around $kL/2\pi = 2.5$ (i.e., $kL/2\pi = 2.5 + \varepsilon/2\pi$ with $\varepsilon/2\pi \ll 1$) enables us to write the transmission coefficient [Eq. (23)] as

$$t = \frac{i\varepsilon(\Delta + \varepsilon a/5)}{-b(\varepsilon + 2\Delta/b) + i\varepsilon(\Delta + \varepsilon a/5)}, \quad (32)$$

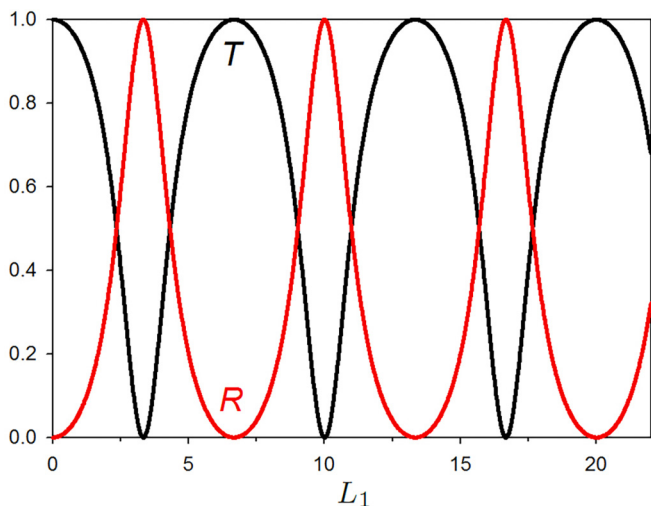


FIG. 7. Variation of the transmittance (black line) and reflectance (red line) vs the stub length L_1 at $kL/2\pi = 3$ and $L = 40$ nm.

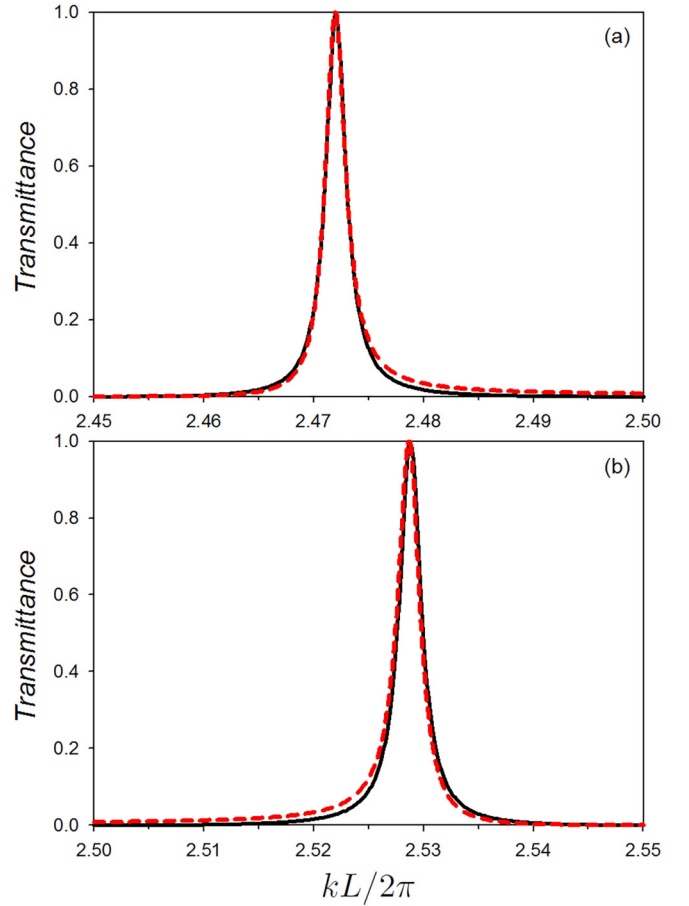


FIG. 8. (a) The solid line presents a zoom plot for the resonance given in Fig. 5(a). The dashed line presents the approximate expression Eq. (33) for $\Delta = 0.03125\pi$. (b) The same as in (a) but for the resonance given in Fig. 5(e) with $\Delta = -0.03125\pi$. The approximate results are in a very good agreement with the exact ones (solid lines) and clearly show that the resonance is of Fano type with $q' \simeq 64.5$ and -64.5 for (a) and (b) respectively and width $2\Gamma \simeq 0.0015$. Notice that the resonance shifts slightly from $kL/2\pi = 2.5$.

where $a = \Delta/\pi + 3/2$, $b = 2\Delta/5\pi + 11/10$, and Δ is the detuning of L_1/L from $3/10$ ($=12/40$) [i.e., $\Delta = 5\pi(L_1/L - 3/10)$].

From Eq. (32), one can show that the transmittance T can be written following the Fano line shape [2] in the form

$$T = B^2 \frac{(\varepsilon - \varepsilon_R + q'\Gamma)^2}{(\varepsilon - \varepsilon_R)^2 + \Gamma^2}, \quad (33)$$

where $B = 2\Delta a/5b^2$, $\Gamma = \Delta^2/b^3$ and $\varepsilon_R = -2\Delta/b$ characterize the width and the position of the resonance, respectively, whereas $q' = 5b^2/2\Delta a$ is the Fano parameter. The results of the approximate expression Eq. (33) are sketched (dashed lines) in Figs. 8(a) and 8(b) for $\Delta = 0.03125\pi$ and -0.03125π respectively. These results are in a very good accordance with the exact ones (solid lines) and clearly show that the resonance is of Fano type with $q' \simeq 64.5$ and -64.5 for Figs. 8(a) and 8(b) respectively and width $2\Gamma \simeq 0.0015$. One can notice that the resonance shifts slightly from $kL/2\pi = 2.5$. Also, q' increases when Δ decreases and tends

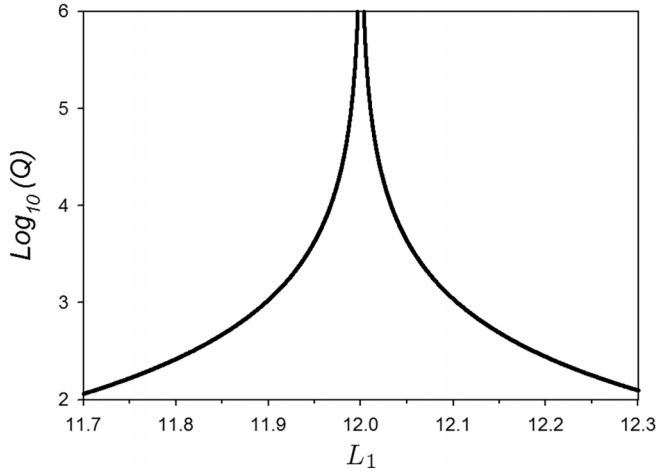


FIG. 9. Variation of the logarithm of the quality factor Q of the peaks reported in Fig. 8 as a function of the stub length L_1 . One can notice that the quality factor of the peak depends on the value of L_1 and as predicted diverges when $L_1 = 12$ nm.

to infinity when Δ vanishes. In this case, the resonance falls at $\varepsilon_R = 0.0$ and its width 2Γ reduces to zero as expected.

In Fig. 9, we have displayed the variation of the logarithm of the quality factor Q of the peaks reported in Fig. 8 as a function of the stub length L_1 . The quality factor Q is defined as the ratio between the central frequency and the full width at half maximum ($Q = 2.5/2\Gamma$). One can notice that the quality factor of the peak depends on the value of L_1 and as predicted diverges when $L_1 = 12$ nm. This result enables us to increase the quality factor of the peaks to infinite values by detuning the length of the stub L_1 . This property is a feature of Fano and induced transparency resonances that does not exist in standard waveguide structures with defect [1]. It should be pointed out that the validity of our results is subject to the requirement that the cross section of the guides is negligible compared to their length and to the propagation wavelength.

V. TRANSMISSION PHASE AND STATE PHASE SHIFT

The transmission phase is obtained from Eq. (23) to be

$$\phi = \tan^{-1} \left(\frac{2S(L/2)C(L_1) + C(L/2)S(L_1)}{2C(L/2)C(L_1)} \right). \quad (34)$$

Another interesting quantity is the first derivative of ϕ with respect to the energy, which is related to the delay time taken by the electrons to traverse the structure. This quantity, called phase time, is defined by [52]

$$\tau_\phi = \hbar \frac{d\phi}{dE}. \quad (35)$$

Moreover, another interesting entity that can be extracted from the Green's function is the bulk state phase shift η . This bulk state phase shift between the final system (the loop and stub with the leads) and the reference system (the isolated loop, the stub, and the two semi-infinite leads) is given by [47]

$$\eta = -\arg[\det\{g^{-1}(M, M)\}]. \quad (36)$$

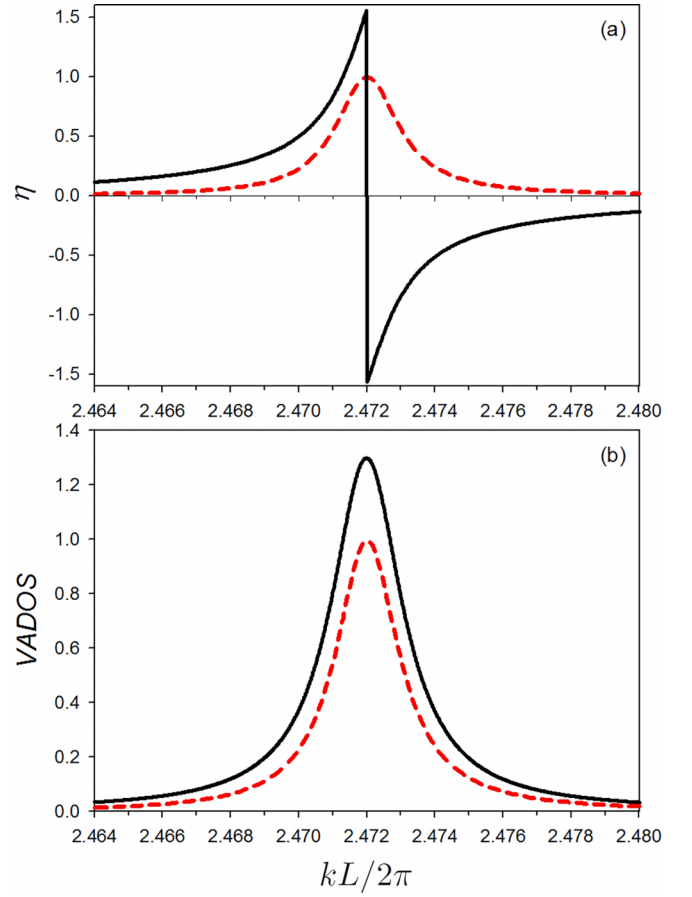


FIG. 10. (a) Bulk state phase shift vs $kL/2\pi$ for the structure presented in Fig. 1(b) with $L = 40$ nm and $L_1 = 12.25$ nm. The Pi drop (at $kL/2\pi \simeq 2.472$) is due to the loss of one bulk state induced by $2S(L/2)C(L_1) + C(L/2)S(L_1) = 0$. This Pi drop is associated with a maximum in the transmittance curve in dashed line, superposed here for agreement check. (b) VADOS vs $kL/2\pi$. The dashed curve recalls the transmittance curve.

From Eq. (22) one can deduce that

$$\eta = -\tan^{-1} \left(\frac{2C(L/2)C(L_1)}{2S(L/2)C(L_1) + C(L/2)S(L_1)} \right). \quad (37)$$

In order to provide an analytical comparison of the density of states with the phases involved in the system, we consider the VADOS $\Delta n(E)$ between the final system depicted in Fig. 1(b) and the reference system composed of the loop, the stub, and the two semi-infinite leads. This quantity is given by [47]

$$\Delta n(E) = -\frac{\hbar}{\pi} \frac{d\eta}{dE}. \quad (38)$$

Note that the Pi drops in ϕ and η are due to the zero values of the denominators appearing in their respective analytical expressions. As these denominators are not the same, the η and ϕ Pi-drop positions are not the same.

In Fig. 10(a) we plot the bulk state phase shift versus the reduced wave vector $kL/2\pi$ for the structure presented in Fig. 1(b) with $L = 40$ nm and $L_1 = 12.25$ nm. The Pi drop (at $kL/2\pi \simeq 2.47$) is due to the loss of one bulk state induced by $[2S(L/2)C(L_1) + C(L/2)S(L_1)] = 0$. This Pi drop

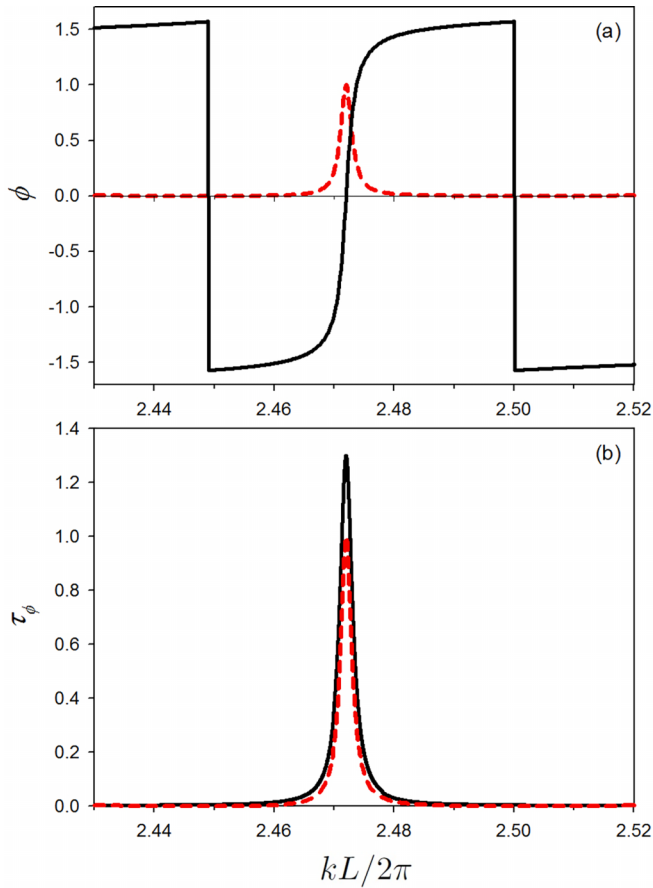


FIG. 11. (a) Transmission phase vs $kL/2\pi$ for the structure presented in Fig. 1(b) with $L = 40$ nm and $L_1 = 12.25$ nm. The Pi drops at $kL/2\pi \simeq 2.45$ and 2.5 are induced by $C(L_1) = 0$ and $C(L/2) = 0$ SIBICs. The transmission phase exhibits a phase jump at the transmission zeros. This provides one single positive peak and two negative delta ones at $kL/2\pi \simeq 2.45$ and 2.5 (not shown), in the phase time. (b) The phase time (in units of $2mL^2/\hbar$) vs the reduced wave vector $kL/2\pi$. The phase time and the VADOS are exactly the same, when one neglects the derivatives of the Pi drops. This happens only when one has two leads. The dashed curve recalls the transmittance one, for agreement checks.

is associated with a maximum in the transmittance curve [Eq. (24)] in dashed line, superposed here for agreement check. Figure 10(b) shows the VADOS versus $kL/2\pi$. The dashed curve recalls the transmittance curve. Let us mention that if we introduced the dissipation in the system by adding a small imaginary part to the energy E , i.e., E becomes $E \pm i(0.0001)$, a negative delta peak will show up in the VADOS plot due to the loss of the bulk state at $kL/2\pi \simeq 2.47$.

Figure 11(a) shows the transmission phase versus the reduced wave vector $kL/2\pi$ for the structure presented in Fig. 1(b) with $L = 40$ nm and $L_1 = 12.25$ nm. The Pi drops at $kL/2\pi \simeq 2.45$ and 2.5 are induced by $C(L_1) = 0$ and $C(L/2) = 0$ SIBICs. The transmission phase exhibits a phase jump at the transmission zeros. This provides one single positive peak and two negative delta ones at $kL/2\pi \simeq 2.45$ and 2.5 (not shown in the plot), in the phase time. Figure 11(b) shows the phase time (in units of $2mL^2/\hbar$) versus $kL/2\pi$. The phase

time and the VADOS are exactly the same, when one neglects the derivatives of the Pi drops. This happens only when one has two leads.

VI. SUMMARY AND PROSPECTIVE

In summary, we have given an analytical evidence about the existence of SIBICs, BICs, and Fano resonances in a 1D monomode electronic structure made of a closed loop of length L , a finite stub of length L_1 , and two semi-infinite leads. A theoretical investigation of the electronic transmittance (reflectance) through this structure using a Green's function method is presented. Numerical results on sharp peaks in detuned waveguides were also reported. These peaks appear as Fano resonances of strong amplitude in the transmittance. The phase time calculations are, in general, different from the variation of the density of states, except for particular cases where the numerator of the transmission coefficient does not vanish or vanishes but without changing sign. In this case, the phase time and the VADOS are equivalent. The quasi-BICs give rise to well defined peaks in the phase time. In addition the structure proposed in this paper exhibits the possibility to tune the quality factors of the induced resonances close to infinity by detuning the length of the stub L_1 . This property is a feature of Fano and EIT resonances and does not exist in standard waveguide structures with defect [1].

The above structure presents a simple example of novel SIBICs. It may be tuned to show very sharp long-lived resonances and antiresonances. The number of the SIBICs and long-lived resonances may be increased by adding more leads and stubs to this structure. This effect may be used for the construction of sharp filters. This paper is also a simple example of how to find all the states, including the SIBIC ones, for any final system. This is achieved with the eigenfunction zeros, the state phase, and the state number conservation between a final system and its reference one. This method is completely general and is expected to be used in future investigations of BIC and SIBIC and their induced long-lived resonances. In addition, the advantage of the simple waveguide electron model presented in this paper consists in finding simple analytical expressions that enable us to discuss the existence of SIBICs, BICs, and Fano resonances as well as the effect of the different stub lengths in tailoring these resonances without incorporating a defect (a dot) in the closed loop, as it is usually the case in such mesoscopic systems [53]. Such a model can also give a qualitative good description of the experimental Fano line shapes in one-dimensional narrow wires at low temperature [54,55]. Let us finally mention that Fano resonances have been studied in single and double asymmetric rings with and without scatters on both arms or in presence of stubs around the loop [41,56–59].

A structure of the considered type (a ringlike electronic microresonator coupled to a finite stub and to two electronic rib/ridge waveguides) can be simulated using commercially available software. Such simulations have to reproduce the above transmission, transmission phase, and phase time results. However, to our knowledge, they are not able to find all the SIBICs, their localization, and their robust zeros.

Indeed the majority of current investigations are done with topological simulation approaches focusing on small

deformations and one BIC. Although introducing the state phase within the numerical routines is not trivial, this is expected to complete and improve simulation results. The knowledge of all system BICs and SIBICs, rather than only one, enables one to choose the better one for a given application. This may help also to use several degenerate strictly bound states for novel devices. Let us finally mention that our theoretical predictions on the generality of the approach must be accompanied by a warning about its limitations. We have dealt with an infinitesimally thin (1D) electronic waveguide without taking into account the cross section of the wires. This leads us to infer that the experimental observation on the moderately thick wires may find a few percent of disagreement with our results, as long as the thickness

is small compared to the length of the wires and to the wavelength.

ACKNOWLEDGMENTS

A.A. gratefully acknowledges the hospitality of the department of Physics, Faculty of Science, Moulay Ismail University of Meknes. This work was partially supported by the program FINCOME “Centre National pour la Recherche Scientifique et Technique, Morocco.” H.A.-W. and E.A.A.-G. gratefully acknowledge the hospitality of the Institut d’Electronique, de Microélectronique et de Nanotechnologie, UMR Centre National de la Recherche Scientifique 8520 and UFR de Physique and Institut Mines-Télécom, UMR 9189 CRIStAL, F-59000, Université de Lille, France.

-
- [1] J. von Neuman and E. Wigner, *Über merkwürdige diskrete Eigenwerte. Über das Verhalten von eigenwerten bei adiabatischen prozessen*, *Phys. Z.* **30**, 467 (1929).
- [2] U. Fano, *Effects of configuration interaction on intensities and phase shifts*, *Phys. Rev.* **124**, 1866 (1961).
- [3] M. Fleischhauer, A. Imamoglu, and J. P. Marangos, *Electromagnetically induced transparency: Optics in coherent media*, *Rev. Mod. Phys.* **77**, 633 (2005).
- [4] J. Jiang, Q. Zhang, Q. Ma, S. Yan, F. Wu, and X. He, *Dynamically tunable electromagnetically induced reflection in terahertz complementary graphene metamaterials*, *Opt. Mater. Express* **5**, 1962 (2015).
- [5] Q. Song, L. Ge, J. Wiersig, and H. Cao, *Formation of long-lived resonances in hexagonal cavities by strong coupling of superscar modes*, *Phys. Rev. A* **88**, 023834 (2013).
- [6] C. W. Hsu, B. Zhen, A. D. Stone, J. D. Joannopoulos, and M. Soljačić, *Bound states in the continuum*, *Nat. Rev. Mater.* **1**, 16048 (2016).
- [7] T. Mrabti, Z. Labdouti, A. Mouadili, E. El Boudouti, and B. Djafari-Rouhani, *Aharonov-Bohm-effect induced transparency and reflection in mesoscopic rings side coupled to a quantum wire*, *Physica E* **116**, 113770 (2020).
- [8] E. N. Bulgakov, K. N. Pichugin, A. F. Sadreev, and I. Rotter, *Bound states in the continuum in open Aharonov-Bohm rings*, *JETP Lett.* **84**, 430 (2006).
- [9] A. A. Bogdanov, K. L. Koshelev, P. V. Kapitanova, M. V. Rybin, S. A. Gladyshev, Z. F. Sadrieva, K. B. Samusev, Y. S. Kivshar, and M. F. Limonov, *Bound states in the continuum and Fano resonances in the strong mode coupling regime*, *Adv. Photonics* **1**, 016001 (2019).
- [10] F. He, J. Liu, G. Pan, F. Shu, X. Jing, and Z. Hong, *Analogue of electromagnetically induced transparency in an all-dielectric double-layer metasurface based on bound states in the continuum*, *Nanomaterials* **11**, 2343 (2021).
- [11] L. Dobrzyński, H. Al-Wahsh, A. Akjouj, and E. A. Abdel-Ghaffar, *Formation and highly directional output of long-lived resonances in photonic comblike structures*, *Phys. Rev. B* **108**, 115426 (2023).
- [12] L. Dobrzyński, H. Al-Wahsh, A. Akjouj, and E. A. Abdel-Ghaffar, *Emergence and highly directed output of long-lived resonances in photonic step ladder structure*, *Opt. Commun.* **548**, 129856 (2023).
- [13] L. Huang, Y. K. Chiang, S. Huang, C. Shen, F. Deng, Y. Cheng, B. Jia, Y. Li, D. A. Powell, and A. E. Miroshnichenko, *Sound trapping in an open resonator*, *Nat. Commun.* **12**, 4819 (2021).
- [14] M. Amrani, I. Quotane, C. Ghouila-Houri, E. H. El Boudouti, L. Krutyansky, B. Piwakowski, P. Pernod, A. Talbi, and B. Djafari-Rouhani, *Experimental evidence of the existence of bound states in the continuum and Fano resonances in solid-liquid layered media*, *Phys. Rev. Appl.* **15**, 054046 (2021).
- [15] A. Mouadili, E. H. El Boudouti, A. Akjouj, H. Al-Wahsh, B. Djafari-Rouhani, and L. Dobrzynski, *Effect of damping on magnetic induced resonances in cross waveguide structures*, *J. Supercond. Novel Magn.* **34**, 597 (2021).
- [16] S. Sun, Y. Ding, H. Li, P. Hu, C.-W. Cheng, Y. Sang, F. Cao, Y. Hu, A. Alù, D. Liu, Z. Wang, S. Gwo, D. Han, and J. Shi, *Tunable plasmonic bound states in the continuum in the visible range*, *Phys. Rev. B* **103**, 045416 (2021).
- [17] Z. Qi, G. Hu, B. Liu, Y. Li, C. Deng, P. Zheng, F. Wang, L. Zhao, and Y. Cui, *Plasmonic nanocavity for obtaining bound state in the continuum in silicon waveguides*, *Opt. Express* **29**, 9312 (2021).
- [18] S. Xie, S. Xie, J. Zhan, C. Xie, G. Tian, Z. Li, and Q. Liu, *Bound states in the continuum in a t-shape nanohole array perforated in a photonic crystal slab*, *Plasmonics* **15**, 1261 (2020).
- [19] S. T. Ha, Y. H. Fu, N. K. Emani, Z. Pan, R. M. Bakker, R. Paniagua-Domínguez, and A. I. Kuznetsov, *Directional lasing in resonant semiconductor nanoantenna arrays*, *Nat. Nanotechnol.* **13**, 1042 (2018).
- [20] L. L. Doskolovich, E. A. Bezus, and D. A. Bykov, *Integrated flat-top reflection filters operating near bound states in the continuum*, *Photon. Res.* **7**, 1314 (2019).
- [21] X. Cui, H. Tian, Y. Du, G. Shi, and Z. Zhou, *Normal incidence filters using symmetry-protected modes in dielectric subwavelength gratings*, *Sci. Rep.* **6**, 36066 (2016).
- [22] F. Wu, J. Wu, Z. Guo, H. Jiang, Y. Sun, Y. Li, J. Ren, and H. Chen, *Giant enhancement of the Goos-Hänchen shift assisted by quasibound states in the continuum*, *Phys. Rev. Appl.* **12**, 014028 (2019).
- [23] D. Conteduca, I. Barth, G. Pitruzzello, C. P. Reardon, E. R. Martins, and T. F. Krauss, *Dielectric nanohole array metasurface for high-resolution near-field sensing and imaging*, *Nat. Commun.* **12**, 3293 (2021).

- [24] K. Koshelev, S. Lepeshov, M. Liu, A. Bogdanov, and Y. Kivshar, Asymmetric metasurfaces with high- q resonances governed by bound states in the continuum, *Phys. Rev. Lett.* **121**, 193903 (2018).
- [25] S. Li, C. Zhou, T. Liu, and S. Xiao, Symmetry-protected bound states in the continuum supported by all-dielectric metasurfaces, *Phys. Rev. A* **100**, 063803 (2019).
- [26] L. Xu, K. Zangeneh Kamali, L. Huang, M. Rahmani, A. Smirnov, R. Camacho-Morales, Y. Ma, G. Zhang, M. Woolley, D. Neshev, and A. E. Miroshnichenko, Dynamic nonlinear image tuning through magnetic dipole quasi-Bic ultrathin resonators, *Adv. Sci.* **6**, 1802119 (2019).
- [27] J. Lee, B. Zhen, S.-L. Chua, W. Qiu, J. D. Joannopoulos, M. Soljačić, and O. Shapira, Observation and differentiation of unique high- q optical resonances near zero wave vector in macroscopic photonic crystal slabs, *Phys. Rev. Lett.* **109**, 067401 (2012).
- [28] C. W. Hsu, B. Zhen, J. Lee, S.-L. Chua, S. G. Johnson, J. D. Joannopoulos, and M. Soljačić, Observation of trapped light within the radiation continuum, *Nature (London)* **499**, 188 (2013).
- [29] E. N. Bulgakov and A. F. Sadreev, Bloch bound states in the radiation continuum in a periodic array of dielectric rods, *Phys. Rev. A* **90**, 053801 (2014).
- [30] L. Huang, B. Jia, A. S. Pilipchuk, Y. Chiang, S. Huang, J. Li, C. Shen, E. N. Bulgakov, F. Deng, D. A. Powell, S. A. Cummer, Y. Li, A. F. Sadreev, and A. E. Miroshnichenko, General framework of bound states in the continuum in an open acoustic resonator, *Phys. Rev. Appl.* **18**, 054021 (2022).
- [31] S. Hein, W. Koch, and L. Nannen, Trapped modes and Fano resonances in two-dimensional acoustical duct-cavity systems, *J. Fluid Mech.* **692**, 257 (2012).
- [32] Y. Sato, Y. Tanaka, J. Upham, Y. Takahashi, T. Asano, and S. Noda, Strong coupling between distant photonic nanocavities and its dynamic control, *Nat. Photon.* **6**, 56 (2012).
- [33] L. Huang, B. Jia, Y. K. Chiang, S. Huang, C. Shen, F. Deng, T. Yang, D. A. Powell, Y. Li, and A. E. Miroshnichenko, Topological supercavity resonances in the finite system, *Adv. Sci.* **9**, 2200257 (2022).
- [34] H. Friedrich and D. Wintgen, Interfering resonances and bound states in the continuum, *Phys. Rev. A* **32**, 3231 (1985).
- [35] L. Huang, L. Xu, M. Rahmani, D. N. Neshev, and A. E. Miroshnichenko, Pushing the limit of high- Q mode of a single dielectric nanocavity, *Adv. Photonics* **3**, 016004 (2021).
- [36] M. V. Rybin, K. L. Koshelev, Z. F. Sadrieva, K. B. Samusev, A. A. Bogdanov, M. F. Limonov, and Y. S. Kivshar, High- Q supercavity modes in subwavelength dielectric resonators, *Phys. Rev. Lett.* **119**, 243901 (2017).
- [37] A. A. Lyapina, D. N. Maksimov, A. S. Pilipchuk, and A. F. Sadreev, Bound states in the continuum in open acoustic resonators, *J. Fluid Mech.* **780**, 370 (2015).
- [38] W. Huang, S. Liu, D. Zeng, Q. Yang, W. Zhang, S. Yin, and J. Han, Coupling-assisted quasi-bound states in the continuum in heterogeneous metasurfaces, *IEEE J. Sel. Top. Quantum Electron.* **29**, 1 (2023).
- [39] X. Zhao, C. Chen, K. Kaj, I. Hammock, Y. Huang, R. D. Averitt, and X. Zhang, Terahertz investigation of bound states in the continuum of metallic metasurfaces, *Optica* **7**, 1548 (2020).
- [40] J. F. Algorri, F. Dell’Olio, P. Roldán-Varona, L. Rodríguez-Cobo, J. M. López-Higuera, J. M. Sánchez-Pena, and D. C. Zografopoulos, Strongly resonant silicon slot metasurfaces with symmetry-protected bound states in the continuum, *Opt. Express* **29**, 10374 (2021).
- [41] M. Amrani, S. Khattou, E. H. El Boudouti, A. Talbi, A. Akjouj, L. Dobrzyński, and B. Djafari-Rouhani, Friedrich-Wintgen bound states in the continuum and induced resonances in a loop laterally coupled to a waveguide, *Phys. Rev. B* **106**, 125414 (2022).
- [42] P. S. Pankin, B. R. Wu, J. H. Yang, K. P. Chen, I. V. Timofeev, and A. F. Sadreev, One dimensional photonic bound states in the continuum, *Commun. Phys.* **3**, 91 (2020).
- [43] F. Wu, X. Qi, M. Qin, M. Luo, Y. Long, J. Wu, Y. Sun, H. Jiang, T. Liu, S. Xiao, and H. Chen, Momentum mismatch driven bound states in the continuum and ellipsometric phase singularities, *Phys. Rev. B* **109**, 085436 (2024).
- [44] L. Dobrzyński, H. Al Wahsh, and A. Akjouj, Photonic open loops, in *Resonance*, Interface Transmission Tutorial Book Series, edited by L. Dobrzyński (Elsevier, Amsterdam, 2023), pp. 1–52.
- [45] L. Dobrzyński, H. Al-Wahsh, A. Akjouj, E. H. El Boudouti, B. Djafari-Rouhani, C. G. Houri, A. Talbi, and G. Lévêque, Photonic paths, in *Photonics*, Interface Transmission Tutorial Book Series, edited by L. Dobrzyński (Elsevier, Amsterdam, 2021), pp. 1–145.
- [46] L. Dobrzyński, A. Akjouj, G. Lévêque, E. H. El Boudouti, and H. Al-Wahsh, Centered system magnons, in *Magnonics*, Interface Transmission Tutorial Book Series, edited by L. Dobrzyński (Elsevier, Amsterdam, 2019), pp. 1–51.
- [47] L. Dobrzyński, A. Akjouj, E. H. El Boudouti, and H. Al-Wahsh *et al.*, Interface response theory, in *Phononics*, Interface Transmission Tutorial Book Series, edited by L. Dobrzyński (Elsevier, Amsterdam, 2018), pp. 1–18.
- [48] E. Schrödinger, An undulatory theory of the mechanics of atoms and molecules, *Phys. Rev.* **28**, 1049 (1926).
- [49] M. Bah, A. Akjouj, and L. Dobrzyński, Response functions in layered dielectric media, *Surf. Sci. Rep.* **16**, 97 (1992).
- [50] H. Al-Wahsh, L. Dobrzyński, and A. Akjouj, Long-lived resonances: Photonic triangular pyramid, *Photonics Nanostruct. Fundam. Appl.* **50**, 101022 (2022).
- [51] L. Dobrzyński, H. Al Wahsh, A. Akjouj, E. H. El Boudouti, C. Ghouila-Houri, A. Talbi, G. Lévêque, and B. Djafari-Rouhani, Closed loop, in *Photonics*, Interface Transmission Tutorial Book Series, edited by L. Dobrzyński (Elsevier, Amsterdam, 2021), pp. 15–19.
- [52] M. Büttiker and R. Landauer, Traversal time for tunneling, *Phys. Rev. Lett.* **49**, 1739 (1982).
- [53] P. Vasilopoulos, O. Kálmán, F. M. Peeters, and M. G. Benedict, Aharonov-Bohm oscillations in a mesoscopic ring with asymmetric arm-dependent injection, *Phys. Rev. B* **75**, 035304 (2007).
- [54] A. Fuhrer, P. Brusheim, T. Ihn, M. Sigrüst, K. Ensslin, W. Wegscheider, and M. Bichler, Fano effect in a quantum-ring-quantum-dot system with tunable coupling, *Phys. Rev. B* **73**, 205326 (2006).
- [55] O. Entin-Wohlman, A. Aharony, Y. Imry, Y. Levinson, and A. Schiller, Broken unitarity and phase measurements in Aharonov-Bohm interferometers, *Phys. Rev. Lett.* **88**, 166801 (2002).

- [56] W.-J. Hsueh, R.-Z. Qiu, and C.-H. Chen, Resonant transport and giant persistent currents in double-asymmetric rings, *Eur. Phys. J. B* **86**, 27 (2013).
- [57] T. Mrabti, Z. Labdouti, O. El Abouti, E. El Boudouti, F. Fethi, and B. Djafari-Rouhani, Transmission gaps, trapped modes and Fano resonances in Aharonov-Bohm connected mesoscopic loops, *Phys. Lett. A* **382**, 613 (2018).
- [58] K.-K. Voo and C. S. Chu, Fano resonance in transport through a mesoscopic two-lead ring, *Phys. Rev. B* **72**, 165307 (2005).
- [59] H. Al-Wahsh, E. H. El Boudouti, B. Djafari-Rouhani, A. Akjouj, and L. Dobrzynski, Transmission gaps and sharp resonant states in the electronic transport through a simple mesoscopic device, *Phys. Rev. B* **75**, 125313 (2007).